Biosensors and Bioelectronics 34 (2012) 171–177

Contents lists available at SciVerse ScienceDirect

Biosensors and Bioelectronics

journal homepage: www.elsevier.com/locate/bios

Direct electrochemistry of novel affinity-tag immobilized recombinant horse heart cytochrome *c*

Florian Schröper[a,b,d], Arnd Baumann[c], Andreas Offenhäusser[a,b], Dirk Mayer[a,b,*]

[a] *Peter Grünberg Institute (PGI-8), Forschungszentrum Jülich, 52425 Jülich, Germany*
[b] *JARA – Fundamentals of Future Information Technology, Forschungszentrum Jülich, 52425 Jülich, Germany*
[c] *Institute of Complex Systems (ICS-4), Forschungszentrum Jülich, 52425 Jülich, Germany*
[d] *Fraunhofer-Institute for Molecular Biology and Applied Ecology IME, 52074 Aachen, Germany*

ARTICLE INFO

Article history:
Received 14 December 2011
Received in revised form 26 January 2012
Accepted 27 January 2012
Available online 7 February 2012

Keywords:
Metalloproteins
Cyclic voltammetry
Bivalent
Histidine tag
Cytochrome *c* reductase

ABSTRACT

During the last decade protein electrochemistry at miniaturized electrodes has become important not only for functional studies of the charge transfer properties of redox proteins but also for fostering the development of sensitive biosensor and bioelectronic devices. One of the major challenges in this field is the directed coupling between electronic and biologically active components. A prerequisite for a fast and reversible electron transfer between electrode and protein is that the protein can be bound to the electrode in a favourable orientation. We examined electrostatic and bioaffinity-tag binding strategies for the directed immobilization of horse heart cytochrome *c* (cyt*c*) on gold electrode surfaces to achieve this goal. Horse heart cyt*c* was expressed in *E. coli* either as non-modified or genetically modified, i.e. histidine (his)-tag containing protein. The his-tags were introduced at defined positions at the N- or C-terminus of the polypeptide. It was our aim to generate tagged-versions of cyt*c* that facilitate strong electronic coupling between protein and electrode and, at the same time, retain their catalytic and regulatory properties. The combination of different immobilization strategies, e.g. his-tag and electrostatic immobilization also opens new avenues for bivalent immobilization of proteins. This is of interest for molecular bioelectronic and biosensing applications where the proteins are immobilized between two crossing electrodes.

1. Introduction

The immobilization of redox active proteins on electrode surfaces and the investigation of charge transfer processes associated with redox enzymes have become increasingly important for the development of novel biosensors and bioelectronic devices with enhanced sensitivity and selectivity (Armstrong and Wilson, 2000; Willner and Katz, 2005; Wu and Hu, 2007; Liu et al., 2010). Especially the development of functionalized electrodes incorporating proteins from biological electron transfer systems is a growing field of research activities due to their promising applicability in innovative chemo- and biosensor devices (Maly et al., 2005; Silveira et al., 2010; Wu et al., 2011; Yagati et al., 2011). One major challenge in protein electrochemistry is to establish efficient electron transfer pathways between the electrode and the immobilized protein while retaining the proteins' functional integrity. This can be achieved by immobilizing the redox protein such that the redox center is in close proximity to the electrode. Since the redox center is central to the enzymatic function such immobilization strategies might lead to a loss of enzymatic activity. In recent years research has largely been concentrated on charge transfer investigations of cytochrome *c* (cyt*c*) as a model system. This redox protein plays a key role in mitochondria, where it acts as an electron shuttle in the respiratory chain and interacts with several essential enzymes. It is thus an ideal protein to study the mechanisms for inter- and intramolecular electron transfer (Imabayashi et al., 1997; Murgida and Hildebrandt, 2008; Song et al., 1993). Numerous electrochemical investigations have focussed on the electron transfer of this redox protein with respect to electrode structure (Leopold and Bowden, 2002; Schröper et al., 2008) and immobilization strategies (Ataka and Heberle, 2003; Hansen et al., 2003; Leopold and Bowden, 2002; Schröper et al., 2010; Song et al., 1993). Various immobilization strategies were investigated to elucidate their influence on charge transfer to and through cyt*c* to identify the most efficient electron transfer conditions. Very good redox responses have been described for cyt*c* electrostatically immobilized on Au electrodes covered with short chain thioalkanoic acids (Avila et al.,

* Corresponding author at: Peter Grünberg Institute (PGI-8), Forschungszentrum Jülich, 52425 Jülich, Germany. Tel.: +49 2461 614023; fax: +49 2461 618733.
E-mail address: dirk.mayer@fz-juelich.de (D. Mayer).

0956-5663/$ – see front matter © 2012 Elsevier B.V. All rights reserved.
doi:10.1016/j.bios.2012.01.039

2000; Protsailo and Fawcett, 2000; Tarlov and Bowden, 1991). In contrast redox activity was reduced when cyt*c* was electrostatically immobilized on long chain thioalcanoic acids and aromatic thiols (Imabayashi et al., 1997). More recently novel immobilization concepts have been developed allowing a directed bifunctional immobilization of redox proteins that holds premise to foster innovative bioelectronical and biosensorical applications. A bifunctional binding of the protein strictly defines its orientation in the junction and thereby directs the charge transfer through a predicted pathway. By this strategy the reliability and reproducibility of a biosensorical device can be improved due to the largely reduced probability of a protein to reorient and thereby perturb the optimal conformation for device operation.

In this manuscript we examined bioaffinity-tag binding strategies for the directed immobilization of horse heart cyt*c* on gold electrode surfaces. We demonstrate the capability of the recombinant proteins to form specific bonds to a gold electrode and gold nanoparticles in parallel. The functional bivalent binding i.e. the electron transfer through tag-tethered cyt*c* and the accessibility of the native binding site for enzymes was examined by an electroenzymatic reaction catalyzed by the enzyme cyt*c* reductase.

2. Materials and methods

2.1. Materials

All chemicals were of high purity grade and used without further purification. Sodium phosphate dibasic dodecahydrate (ultra ≥ 99%), sodium phosphate monobasic monohydrate (ultra ≥ 99.5%), imidazole (≥99.5%), *N*α,*N*α-bis(carboxymethyl)-L-lysine hydrate (ANTA), dithiobis(succinimidylpropionate) (DTSP) and 3-mercaptopropionic acid (MPA, purum ≥ 99%) were purchased from Fluka. Ethanol (purum ≥ 99.8%) and sodium chloride (puriss ≥ 99.8%) were supplied from KMF Laborchemie Handels GmbH (Germany). 11-Mercaptoundecanoic acid (MUA, 95%), ammonium sulphate (≥99.5%), nickel(II) sulphate, Gly–Gly hydrochloride, nicotinamide adenine dinucleotide (NADH) and the proteins cytochrome *c* from equine heart (BioUltra ≥ 99%) and cyt*c* reductase from porcine heart were purchased from Sigma–Aldrich. Construction, expression and purification of recombinant cyt*c* are described in the Supplemental information (SI). All other chemicals were purchased from Sigma–Aldrich. Aqueous solutions were made using ultra-pure water produced by a MilliQ system (Millipore).

2.2. Surface modification

Protein immobilization was performed on Au substrates covered with self-assembled monolayers (SAM). For electrochemical investigations a flame annealed Au (1 1 1) crystal was used, whereas surface plasmon resonance (SPR) measurements were performed by using a glass slide with Au film (15–30 nm) prepared by physical vapour deposition ($n = 1.61$). All Au surfaces were cleaned in sulphuric acid followed by subsequent extensive rinsing with MilliQ water before use. For electrostatic immobilization, the cleaned Au surface was incubated in 10 mM ethanolic solution containing MUA or MPA for at least 5 min and subsequent rinsing with ethanol and MilliQ water. Alternatively the Au surface was functionalized with a NiNTA SAM as described previously (Ataka et al., 2004; Mayer et al., 2005) enabling the immobilization of his-tagged recombinant cyt*c*. The cleaned Au surface was first incubated in 2.5 mM dithiobis(succinimidyl propionate) (DTSP) in DMSO for 15 min, then dried under argon and immersed into a 150 mM *N*(α),*N*(α)-bis(carboxymethyl)-L-lysinehydrate (ANTA) solution (in 0.5 M K_2CO_3 buffer, pH 9.8) for 90 min. Finally the NTA functionalized surface was loaded with Ni^{2+} ions by applying a 50 mM $NiSO_4$ solution for 15 min followed by rinsing with MilliQ water.

2.3. Protein immobilization

The Au (1 1 1) electrodes covered with SAM molecules were incubated in 10 μM cyt*c* solution in 5.78 mM sodium phosphate buffer (pH 7) for at least 5 min (electrostatic binding) and 60 min (tag immobilization), respectively, followed by a rinsing step to remove unbound protein. Alternatively, protein adsorption was monitored by in situ SPR using a flow cell configuration and a Kretschmann-type spectrometer (BIOSUPLAR 3, Mivitec GmbH, Germany, $\lambda = 670$ nm). The absorption process occurring at the solid–liquid interface can be monitored in real time, by selecting an appropriate angle of incidence θ and monitoring the reflected intensity as a function of time. Knowledge of the shape of the resonance curve enabled interpretation of the reflected intensity as a shift of the angle of resonance. The flow rate of sample injection and rinsing was controlled at 0.256 ml/min with a pump (REGLO Digital, ISMATEC, Switzerland).

2.4. Atomic force microscopy

All atomic force microscopy (AFM) measurements were performed in tapping mode at room temperature with a MultiMode AFM/STM (Bruker, Santa Barbara, CA) equipped with a Nanoscope-IV controller and a 15 μm scanner. Commercially available silicon cantilevers have been employed with resonance frequencies between 260 and 300 kHz.

2.5. Cyclic voltammetry

The redox behaviour of immobilized cyt*c* was investigated by cyclic voltammetry using an EG&G 283 Potentiostat (Princeton Applied Research, Princeton, NJ, USA). Au (1 1 1) electrodes were prepared by flame annealing and incubation in ethanolic SAM solution followed by protein immobilization as described above. Before starting the electrochemical recording the cyt*c* covered electrodes were thoroughly rinsed with buffer to remove unbound protein. Cyclic voltammograms (CV) were recorded under argon atmosphere in 5.78 mM sodium phosphate buffer at pH 7. A platinum wire and a Ag/AgCl electrode (3 M KCl) were employed as counter (CE) and reference electrodes (RE), respectively. All potentials are quoted versus the Ag/AgCl potential. The crystal was immersed to the electrolyte in a hanging meniscus configuration. The electroenzymatic reaction was initiated by injection of 0.8 mg/ml cyt*c* reductase and 7.5 mM NADH (Sigma–Aldrich).

3. Results and discussion

3.1. Genetically modified his-tagged cyt*c*

Cloning of the recombinant his-tagged cyt*c* variants was successful and confirmed by sequencing (data not shown). In total four cyt*c* constructs were expressed. These included pJRhrsN2 (Rumbley et al., 2002) coding for wildtype cyt*c* and the modified variants pJRhrsN2-Chis, pJRhrsN2-Nhis and pJRhrsN2-NChis coding for affinity-tagged cyt*c* constructs with either a C-terminal (C-his), N-terminal (N-his) or bifunctional (NC-his) hexahistidine tags (Fig. 1A). Yields of *E. coli* expressed and purified recombinant cyt*c* were ≈3 mg/L for wildtype cyt*c* and up to 12 mg/L for his-tagged proteins. All purified samples were checked and compared to commercially available cyt*c* by Coomassie-stained SDS-gels as exemplarily shown in Fig. 1B for cyt*c* (NC-his). In this example a

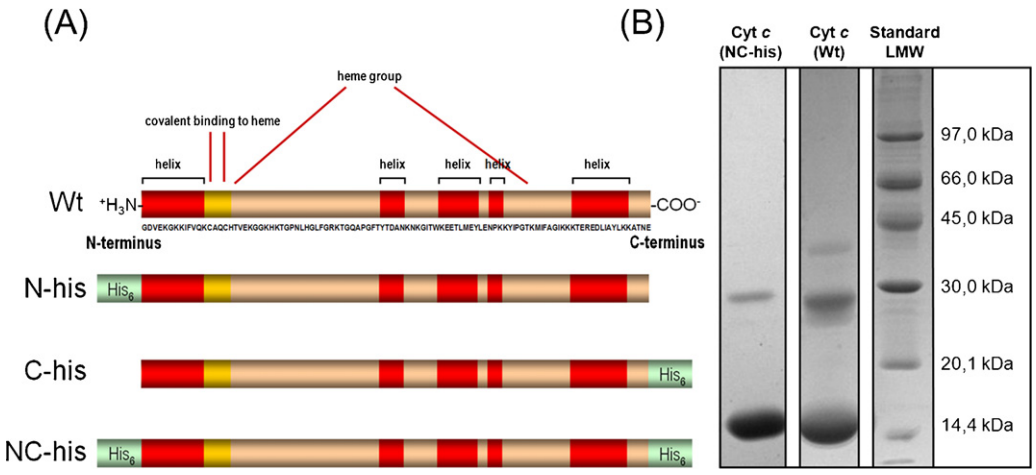

Fig. 1. (A) Pictogram of horse heart cyt*c* (Wt). The amino acid sequence is given in the one letter code. The three recombinant cyt*c* constructs with C- and/or N-terminal his-tag are also displayed. (B) Coomassie stained SDS polyacrylamide gels of purified his-tagged cyt*c* and commercially available horse heart cyt*c*. For comparison a low molecular weight (LMW) standard was used.

protein of approximately 14 kDa was enriched in the eluate. Two protein bands of higher molecular weight most likely are dimeric and trimeric forms of cyt*c* (Fig. 1B).

3.2. Investigation of functionality

Due to their intrinsic heme group, chromo proteins like cyt*c* can be characterized by UV/vis absorption spectroscopy which exhibit heme-characteristic absorption bands (Will et al., 1983). Absorption spectra of oxidized and reduced cyt*c* show significant differences, experimental details are described at SI. Oxidized cyt*c* has two absorption bands at 410 nm (Soret band) and 530 nm. In its reduced form the Soret band shifts to 416 nm, the 530 nm band disappears whereas two additional bands appear at 520 nm and 550 nm (Margoliash and Walasek, 1967). All purified proteins were analyzed by UV/vis adsorption spectroscopy in the range between 380 nm and 600 nm to control for correct heme loading and functionality. A comparison to commercially available cyt*c* in the reduced form (Fig. 2A) revealed that all samples resulted in almost identical spectra. As an example the adsorption bands at 416 nm, 520 nm and 550 nm for purified cyt*c* (NC-his) are shown in Fig. 2A. From this result a correct heme loading can be concluded for all recombinant cyt*c* types. Variations in peak height are attributed to differences in cyt*c* concentration. Functional integrity was also investigated by a photochemical enzyme test utilizing cyt*c* reductase. Therefore, cyt*c* was oxidized chemically by adding potassium hexacyanoferrate (III). The UV/vis spectrum was recorded revealing two bands at 410 nm and 530 nm. Addition of cyt*c* reductase (0.005–0.025 U; porcine heart; Sigma–Aldrich) and NADH (1 mM; Sigma–Aldrich) led to a change in the absorption spectrum within five minutes due to the formation of the reduced form of cyt*c* (Fig. 2B). The native enzymatic conversion from oxidized cyt*c* to its reduced form could be observed for all his-tagged cyt*c* constructs as reported previously for cys-tagged cyt*c* variants (Schröper et al., 2010). Thus all recombinant cyt*c* constructs were accessible for cyt*c* reductase and no significant difference can be observed between the enzymatic reduction of native cyt*c* and recombinant protein. Therefore, it can be assumed that all recombinant proteins were fully functional.

3.3. Immobilization studies

Electrostatic binding as well as affinity tag binding of recombinant his-tagged cyt*c* on modified Au surfaces was investigated by SPR and compared to the results gained for commercial non-modified cyt*c* (Fig. 3). Electrostatic binding of commercial Wt cyt*c* was fast, showed Langmuir adsorption behaviour and resulted in a stable surface coverage in less than 10 min as can be seen from the black curve in Fig. 3A. Rinsing with buffer caused no significant protein desorption. Electrostatic binding of his-tagged cyt*c* was also successful leading to a stable coverage, although binding kinetic was slower (≥20 min). For all three his-tagged constructs significant differences in the SPR experiments were observed (Fig. 3A) leading to deviant Δreflectivity values and correlated with an increased surface coverage compared to non-modified cyt*c*. These observations suggest different immobilization behaviour(s) and most likely the formation of protein films with thicknesses exceeding monolayers due to the additional his-tags. Interestingly, higher surface coverage could not be explained by unspecific binding since rinsing with buffer did not cause significant desorption. The formation of such aggregates might be caused by coordination of metal ions to histidines of neighbouring proteins. The observed coverage also differed with respect to the number and position of the his-tags, since sterical effects of the tags result in different protein binding configurations. Immobilization of his-tagged cyt*c* on NiNTA modified Au surfaces was also monitored by SPR (Fig. 3B). In all cases binding via the his-tag was successful and showed fast adsorption behaviour typical for self-assembled monolayers and leading to almost identical surface coverage. For cyt*c* (N-his) the fastest binding was observed saturating within 15 min, whereas cyt*c* (C-his) binding saturated after approximately 25 min, indicating differences in the binding kinetics. As a result, an interference of two competing binding events can be assumed for cyt*c* (NC-his) (>30 min), which decelerates the binding of further incoming proteins. Unspecific interactions were not observed for any affinity-tag binding. The SPR measurements revealed that all recombinant proteins could be immobilized either by electrostatic immobilization or via their affinity-tags leading to stable protein coverage. Bifunctional immobilization of recombinant cyt*c* was investigated by using Au nanoparticles (AuNP) with a diameter of 5 nm which were functionalized by carboxylic groups. First cyt*c* was immobilized via the affinity-tag and monitored by SPR as described previously (Fig. 3B). After protein binding saturated the sample was shortly rinsed before in a second step AuNP solution (5 nm citrated gold colloid suspension, Sigma–Aldrich; 1:1 diluted in sodium phosphate buffer) was applied to the surface. This led to a second electrostatic binding event of the citrated nanoparticles ontop of the tag-tethered cyt*c* (Fig. 3C), whereas AuNP did not show any

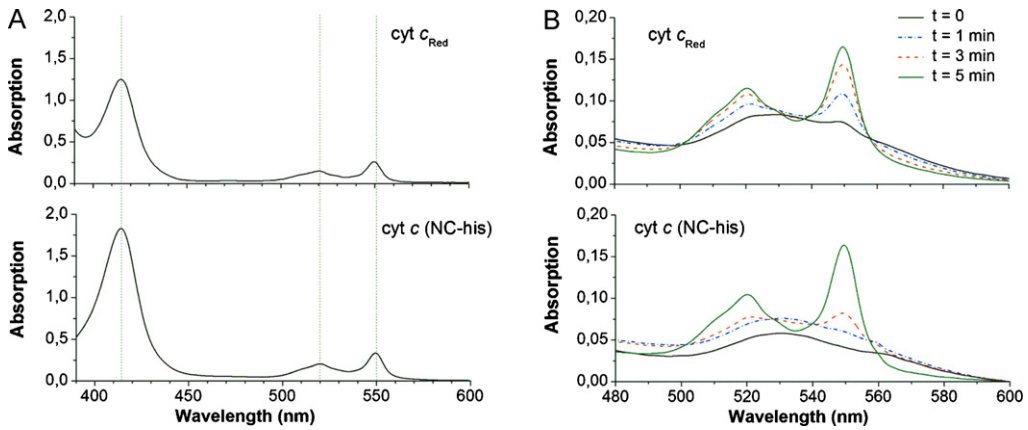

Fig. 2. (A) UV/vis spectra of purified his-tagged recombinant cyt*c* in comparison to commercially available wildtype horse heart cyt*c* in reduced form. (B) UV/vis spectra of the same cyt*c* in chemically oxidized state (black curve) and 1 min, 3 min, and 5 min after the addition of cyt*c* reductase and NADH.

binding to the NiNTA covered surface without cyt*c* (data not shown). Binding of AuNPs was independently confirmed by AFM measurements (Fig. 3D and E). The NiNTA functionalized surface covered with his-tagged cyt*c* (N-his) (Fig. 3D) was incubated in nanoparticle solution for 15 min followed by rinsing in MilliQ water. Fig. 3E shows the sample from Fig. 3D but now completely covered with the 5 nm particles (surface coverage ~80%).

3.4. Electrochemistry

The redox activity of immobilized recombinant his-tagged cyt*c* and native cyt*c* was investigated by cyclic voltammetry. Commercial Wt cyt*c* was immobilized electrostatically on a Au (1 1 1) electrode modified with MUA and CVs were recorded at 100 mV/s as described above. Defined oxidation and reduction peaks positioned at 0 mV (Ag/AgCl) with no peak separation are consistent with published data (Song et al., 1993). A surface coverage of $B_n = 66\%$ redox active protein was calculated from the mean charge density σ_m (Table 1). Interestingly, his-tagged cyt*c* electrostatically immobilized on MUA did not show any redox signal as illustrated exemplarily for cyt*c* (C-his) in Fig. 4A (dashed curve). We assume that the his-tag prevents electron transfer, independent from its position at the N- or C-terminus of the protein. On the contrary, immobilization of these proteins on Au (1 1 1) covered with a short chain length MPA SAM resulted in a clear electrochemical signal (Fig. 4A; green curve). Here the lower distance between electrode surface and redox center enables an efficient electron transfer. However, the separation of the oxidation and reduction peaks (~80 mV) indicated a kinetic limitation as it is usually known for long chain molecules and thus far distance electron transfer (Avila

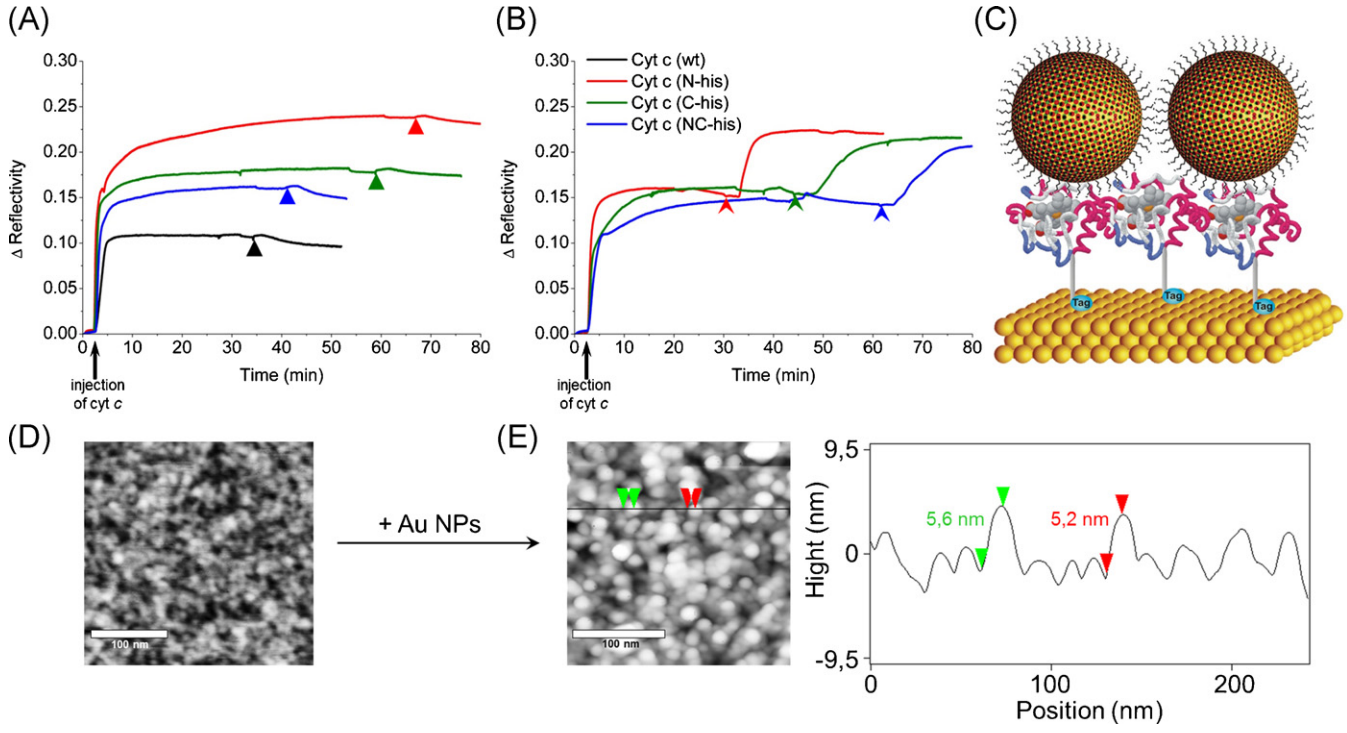

Fig. 3. (A) SPR diagrams for electrostatically immobilized wildtype cyt*c* in comparison to electrostatically immobilized his-tagged cyt*c* (C-his, N-his, NC-his). Arrows heads (▲) mark the starting point for rinsing with buffer. (B) SPR diagrams for his-tag binding of recombinant cyt*c*. Arrows heads (▲) mark the injection of —COOH functionalized AuNPs. (C) Schematic view of the electrostatically immobilized AuNPs ontop of cyt*c*. (D) Tapping mode AFM image of a Au (1 1 1) surface covered with his-tag immobilized cyt*c* (N-his) before and (E) after incubation in AuNP solution.

Table 1
Electrochemical data for electrostatically and affinity-tag immobilized cyt*c* constructs on Au (1 1 1) covered with variable SAMs. Data were determined from cyclic voltammograms recorded with 100 mV/s. Data for cyt*c* (C-cys) was published before (Schröper et al., 2010) and is given for comparison.

	E_0 [mV]	ΔE [mV]	σ_m [μC/cm^2]	B_n [%]
Cyt*c* (Wt) MUA	0	8	1.09	66
Cyt*c* (C-his) MPA	−1	82	0.44	27
Cyt*c* (C-cys) MUA	5	8	0.91	54
Cyt*c* (C-his) NiNTA	54	44	0.20	12
Cyt*c* (N-his) NiNTA	74	36	0.07	4
Cyt*c* (NC-his) NiNTA	59	38	0.11	6
Cyt*c* (C-cys) MPhOH	69	59	1.26	75

et al., 2000; Feng et al., 1997; Niki et al., 2002; Yue and Waldeck, 2005; Yue et al., 2008). Thus it could be assumed that the distance between electrode and redox center of all his-tagged cyt*c* constructs was larger than for native cyt*c*. Electron transfer could only be achieved when short chain length SAM molecules, like MPA, were used for immobilization. A crucial aspect of this work was to produce and purify recombinant cyt*c* that can be immobilized via its affinity tag while still enabling electron transfer. Therefore, all his-tagged cyt*c* constructs were immobilized on NiNTA functionalized Au (1 1 1) electrodes as described above and CVs were recorded. For all three constructs stable redox peaks with slight peak separation were observed (see Fig. 4B) which confirmed reversible surface-confined charge transfer. Cyt*c* (C-his) yielded the strongest redox

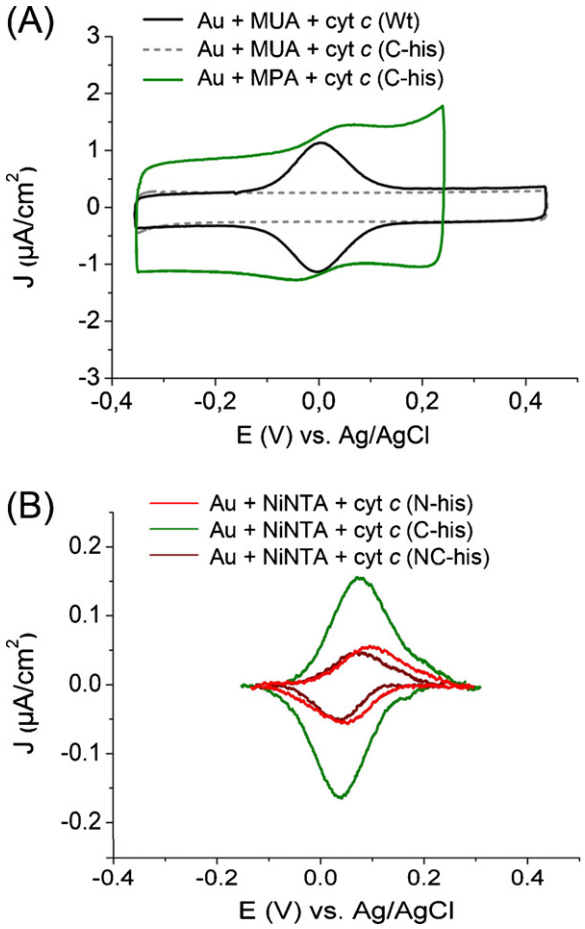

Fig. 4. Cyclic voltammograms of (A) electrostatically immobilized his-tagged cyt*c* in comparison to wildtype cyt*c* (black curve) and (B) recombinant cyt*c* samples immobilized via their his-tag on a NiNTA functionalized Au (1 1 1) electrode at a scan rate of 100 mV/s. (For interpretation of the references to colour in this figure legend, the reader is referred to the web version of this article.)

signal whereas cyt*c* with N-terminal his-tag and the combined NC-terminal tags showed less pronounced redox activity. This might be explained by the proximity of the C-terminus and one of the main electron transfer pathways through cyt*c* (Willner and Katz, 2005). Peak potentials were shifted to more positive potentials, indicating a structural influence of the immobilization strategy on heme coordination and thus redox potential. A similar observation has been described by Murgida and Hildebrandt (2008). They showed the existence of two conformational isomers. In the native form an axial histidine and a methionine coordinate the heme iron. The second isomer lacks the methionine binding due to an electrostatic gating effect. The interfacial electric field of short chain carboxylic monolayers induces a rapture of the relatively weak methionine coordination, which is accompanied by a cathodic shift of the redox potential. This assumption was supported by the potential differences between proteins immobilized via electrostatic interactions and affinity-tags, studied in this work.

The cyclic voltammograms revealed a separation of the anodic and cathodic peak in the range of 40 mV, indicating a kinetic limitation of the electron transfer. In contrast to the electrostatic immobilization it can be assumed that affinity-tag binding leads to a non-conformal orientation and thus an increased mean distance between electrode and heme group. Considering the geometric dimension of cyt*c* ($d \approx 3.5$ nm) (Louie and Brayer, 1990) and an assumed maximum surface concentration of 19 pmol (Heering et al., 2004) we calculated from the charge densities surface coverages B_n of ≈2% for cyt*c* (C-his) and of approx. 5% for the other two constructs. These values are similar to those reported by Heering et al. (2004) for YCC immobilized via Cys102. Since SPR and AFM measurements revealed a densely covered surface these low values compared to the electrostatic binding can be attributed to immobilized cyt*c* which does not contribute to the charge transfer. Such behaviour might be explained by an inhomogeneous orientation of cyt*c* molecules on the electrode surface leading to variable distances between heme and electrode. As a consequence only a fraction of all proteins obtained an orientation enabling electron transfer. For cyt*c* (C-his) the charge transfer was favoured due to the proximity between the his-tag and the intramolecular electron transfer pathway (Willner and Katz, 2005). Taken together, we can conclude that a reversible electron transfer between electrode and his-tagged cyt*c* is more pronounced for C-terminal cyt*c* (C-his) than for cyt*c* (NC-his) and (N-his). Comparing these results to the findings reported for cys-tagged cyt*c* (Schröper et al., 2010) it is noteworthy that charge density and thus, contribution of surface molecules to the electrochemical signal is more pronounced for cys-tag binding than for his-tag binding. This might be explained by the higher conformation flexibility of ion-based binding via NiNTA in comparison to rather ridged bonds of peptides (cys-tag) and electrostatic binding (wildtype). Therefore, ridged bonds may provide a more firm and efficient electronic coupling between electrode and protein.

Functionality of immobilized redox proteins and the ability of catalytic electron transfer is a major challenge for prospective applications in the field of biosensors or molecular bioelectronics. Previous studies focusing on electroenzymatic interactions between cyt*c* and enzymes like cyt*c* oxidase (Haas et al., 2001), cyt*c* peroxidase, cd_1 nitrite reductase and nitric oxide reductase (Heering et al., 2004) pointed out the importance to ensure native enzyme binding facilitating reproducible electron relay when cyt*c* was immobilized on the electrode surface. Electrostatically immobilized cyt*c* was unable to interact with solved cyt*c* oxidase because the binding site of cyt*c* is located in a lysine rich domain facing the electrode (Koppenol and Margoliash, 1982). To overcome this constrain alternative binding sites were explored. The use of native (Heering et al., 2004) or recombinant engineered cysteine binding sites (Schröper et al.,

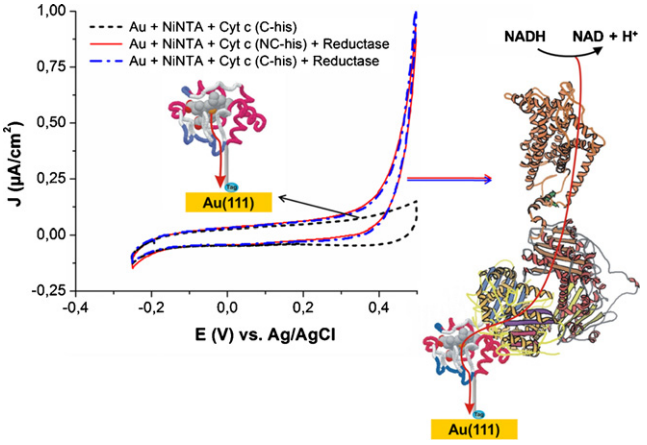

Fig. 5. Cyclic voltammograms of his-tag immobilized cyt*c* (black cuve) and electroenzymatic reaction catalyzed by cyt*c* reductase (red and blue curves), recorded with a scan rate of 2 mV/s. Protein structures were taken from the RCSB Protein Data. (For interpretation of the references to colour in this figure legend, the reader is referred to the web version of this article.)

2010) in the C-terminal region of cyt*c* demonstrated the suitability of such alternative immobilization strategies to ensure enzymatic functionality. To verify the potential applicability of the recombinant his-tag immobilized cyt*c*, its capability to relay electrons to enzymes was studied according to Haas et al. (2001). Since we demonstrated above that our recombinant cyt*c* could be reduced by cyt*c* reductase in solution, this enzyme was now employed to interact electrochemically with cyt*c* immobilized via its his-tag to the NiNTA functionalized electrode. CVs of the electroenzymatic reaction of surface tethered proteins showed stable redox signals as described above (2 mV/s, Fig. 5). Instantaneously after injection of porcine heart cyt*c* reductase (0.8 mg/ml) and 7.5 mM NADH the redox response changed significantly. A strong increase of the oxidative current as it is typical for electroenzymatic reactions (Willner and Katz, 2005) was observed for all his-tagged constructs. Fig. 5 shows the CV exemplary for cyt*c* (C-his) (blue curve) and cyt*c* (NC-his) (red curve). CVs of cyt*c* (N-his) had almost identical shape and peak height confirming the electroenzymatic applicability of all constructs. The increasing anodic current can be explained by the recurring process of enzymatic reduction and electrochemical oxidation where electrons are transferred from NADH via cyt*c* reductase to the heme group of cyt*c*. Here, electrons were directly transferred from the reduced cyt*c* to the electrode driven by the applied potential. This resulted in an oxidized form of cyt*c* which could then be reduced enzymatically again. As described for coupled electrochemical reactions, the redox peaks observed for cyt*c* reductase free cyt*c* (Fig. 4) vanishes for the enzyme linked system due the permanent relay of electrons through the immobilized cyt*c* (Bard and Faulkner, 2001). The moderate increase of the electrocatalytic current implies a kinetic limitation in enzymatic turnover. Such behaviour is quite evident due to the higher molecular weight of cyt*c* reductase compared to the small immobilized cyt*c* molecules and might be explained by diffusional and/or steric limitations in enzyme binding. We also immobilized cyt*c* electrostatically before injection of reductase and were not able to detect any catalytic response. This result confirms the findings of Haas et al. (2001) who used cyt*c* oxidase instead of cyt*c* reductase. In both cases electron relay cannot take place because both enzymes, i.e. cyt*c* oxidase and cyt*c* reductase, need to bind to the same lysine rich domain of cyt*c* (Koppenol and Margoliash, 1982) which is buried when cyt*c* is immobilized electrostatically.

4. Conclusion

In conclusion we succeeded to express and purify three versions of fully functional his-tagged recombinant cyt*c* that could be used for bifunctional immobilization on electrode surfaces. We were able to demonstrate that all three cyt*c* constructs could be successfully immobilized to an electrode surface either by electrostatic immobilization or via its his-tag. Immobilization via the C-terminal his-tag enabled most efficient electron transfer due to the proximity between C-terminus and the major electron transfer path. Furthermore, we were able to demonstrate that his-tag immobilized cyt*c* was able to functionally interact with its native effector enzyme cyt*c* reductase as well as to bind to surfaces of solids like AuNPs. With an electroenzymatic experiment we also demonstrated the alternating electron transfer between electrode and effector enzyme via the immobilized cyt*c* molecule. Proteins with the capability to perform selective bivalent binding to different biological or inorganic partners are of special interest for molecular bioelectronics because they facilitate an oriented assembly of functionally linked biomolecules and solid device components in predictable fashion. By this means, such proteins may advance the development of novel biosensing devices where direct enzymatic charge transfer is required between electrode and enzyme. Furthermore, devices can be envisioned where electroactive proteins are immobilized in an oriented fashion between two crossing electrodes or bridging a nanosized gap between two nanoelectrodes.

Acknowledgements

We are grateful to Dr. Jon Rumbley (UMinn, Duluth) for providing the pJRhrsN2 and pJRopti1 expression vectors coding for recombinant horse heart cyt*c*. The Volkswagen Stiftung (Grant no. I77–116) is kindly acknowledged for financial support.

Appendix A. Supplementary data

Supplementary data associated with this article can be found, in the online version, at doi:10.1016/j.bios.2012.01.039.

References

Armstrong, F.A., Wilson, G.S., 2000. Electrochim. Acta 45, 2623–2645.
Ataka, K., Heberle, J., 2003. J. Am. Chem. Soc. 125, 4986–4987.
Ataka, K., Giess, F., Knoll, W., Naumann, R., Haber-Pohlmeier, S., Richter, B., Heberle, J., 2004. J. Am. Chem. Soc. 126, 16199–16206.
Avila, A., Gregory, B.W., Niki, K., Cotton, T.M., 2000. J. Phys. Chem. B 104, 2759–2766.
Bard, A.J., Faulkner, L.F., 2001. Electrochemical Methods. John Wiley & Sons, New York, 496.
Feng, Z.Q., Imabayashi, S., Kakiuchi, T., Niki, K., 1997. J. Chem. Soc. Faraday Trans. 93, 1367–1371.
Haas, A.S., Pilloud, D.L., Reddy, K.S., Babcock, G.T., Moser, C.C., Blasie, J.K., Dutton, P.L., 2001. J. Phys. Chem. B 105, 11351–11362.
Hansen, A.G., Boisen, A., Nielsen, J.U., Wackerbarth, H., Chorkendorff, I., Andersen, J.E.T., Zhang, J., Ulstrup, J., 2003. Langmuir 19, 3419–3427.
Heering, H.A., Wiertz, F.G.M., Dekker, C., de Vries, S., 2004. J. Am. Chem. Soc. 126, 11103–11112.
Imabayashi, S., Iida, M., Hobara, D., Feng, Z.Q., Niki, K., Kakiuchi, T., 1997. J. Electroanal. Chem. 428, 33–38.
Koppenol, W.H., Margoliash, E.J., 1982. Biol. Chem. 257, 4426–4437.
Leopold, M.C., Bowden, E.F., 2002. Langmuir 18, 2239–2245.
Liu, Y., Offenhäusser, A., Mayer, D., 2010. Biosens. Bioelectron. 25, 1173–1178.
Louie, G.V., Brayer, G.D., 1990. J. Mol. Biol. 214, 527–555.
Maly, J., Masojidek, J., Masci, A., Ilie, M., Cianci, E., Foglietti, V., Vastarella, W., Pilloton, R., 2005. Biosens. Bioelectron. 21 (6), 923–932.
Margoliash, E., Walasek, O.F., 1967. Methods Enzymol. 10, 339–348.
Mayer, D., Ataka, K., Heberle, J., Offenhäusser, A., 2005. Langmuir 21, 8580–8583.
Murgida, D.H., Hildebrandt, P., 2008. Chem. Soc. Rev. 37, 937–945.
Niki, K., Sprinkle, J.R., Margoliash, E., 2002. Bioelectrochemistry 55, 37–40.
Protsailo, L.V., Fawcett, W.R., 2000. Electrochim. Acta 45, 3497–3505.
Rumbley, J.N., Hoang, L., Englander, S.W., 2002. Biochemistry 41, 13894–13901.
Schröper, F., Brüggemann, D., Mourzina, Y., Wolfrum, B., Offenhäusser, A., Mayer, D., 2008. Electrochim. Acta 53, 6265–6272.

Schröper, F., Baumann, A., Offenhäusser, A., Mayer, D., 2010. Chem. Commun. 46, 5295–5297.
Silveira, C.M., Gomes, S.P., Araujo, A.N., Montenegro, M.C.B.S.M., Todorovic, S., Viana, A.S., Silva, R.J.C., Moura, J.J.G., Almeida, M.G., 2010. Biosens. Bioelectron. 25 (9), 2026–2032.
Song, S., Clark, R.A., Bowden, E.F., Tarlov, M.J., 1993. J. Phys. Chem. 97, 6564–6572.
Tarlov, M.J., Bowden, E.F., 1991. J. Am. Chem. Soc. 113, 1847–1849.
Will, O.H., Ruddat, M., Garber, E.D., 1983. Curr. Microbiol. 8, 23–26.
Willner, I., Katz, E., 2005. Bioelectronics. Wiley-VCH, Weinheim.
Wu, Y., Hu, S., 2007. Microchim. Acta 159, 1–17.
Wu, Y.H., Liu, X.Q., Zhang, L., Wang, C.T., 2011. Biosens. Bioelectron. 26 (5), 2177–2182.
Yagati, A.K., Lee, T., Min, J., Choi, J.W., 2011. Bioelectrochemistry 80 (2), 169–174.
Yue, H., Waldeck, D.H., 2005. Curr. Opin. Solid State Mater. Sci. 9, 28–36.
Yue, H., Waldeck, D.H., Schrock, K., Kirby, D., Knorr, K., Switzer, S., Rosmus, J., Clark, R.A., 2008. J. Phys. Chem. C 112, 2514–2521.